

# Decay Rate of Triaxially-Deformed Proton Emitters

Cary N. Davids and Henning Esbensen

*Physics Division, Argonne National Laboratory, Argonne, IL 60439*

(Dated: November 13, 2018)

## Abstract

The decay rate of a triaxially-deformed proton emitter is calculated in a particle-rotor model, which is based on a deformed Woods-Saxon potential and includes a deformed spin-orbit interaction. The wave function of the  $I = 7/2^-$  ground state of the deformed proton emitter  $^{141}\text{Ho}$  is obtained in the adiabatic limit, and a Green's function technique is used to calculate the decay rate and branching ratio to the first excited  $2^+$  state of the daughter nucleus. Only for values of the triaxial angle  $\gamma < 5^\circ$  is good agreement obtained for both the total decay rate and the  $2^+$  branching ratio.

PACS numbers: 21.10.Tg, 23.50.+z, 27.60.+j

## I. INTRODUCTION

The fundamental simplicity of the proton decay process in nuclides whose ground states are unstable to proton emission has enabled a good deal of nuclear structure information to be obtained on nuclei beyond the proton drip line [1]. The observable quantities are the proton energies and half-lives. In the rare-earth region, the proton emitters are predicted to have large static quadrupole deformations [2]. For these cases, analysis of the measurements has been carried out using a particle-rotor model, with the unbound proton interacting with an axially-symmetric deformed core [3, 4, 5, 6, 7, 8, 9, 10, 11]. The results of such analyses over the past several years has been to obtain a good description of the ground-state properties of deformed rare-earth proton emitters, including deformations, occupation factors, Nilsson orbitals for the decaying protons, and wave function decompositions.

Adding to the information provided by the observation of decay protons, recent measurements have been made of the level structure of the deformed proton emitter  $^{141}\text{Ho}$  by means of in-beam  $\gamma$ -ray spectroscopy [12]. Particle-rotor calculations of the energy levels in the rotational band lying above the  $I = 7/2^-$  ground state suggest that better agreement with experiment would be obtained if the nuclear shape possessed a small amount of static triaxial deformation [12]. From the standpoint of proton radioactivity it is therefore of interest to investigate the effect of a static triaxial deformation on the decay rate of a deformed proton emitter. In this work we present such an analysis, and obtain numerical results for the decay rate of the deformed proton emitter  $^{141g}\text{Ho}$ .

## II. COUPLED EQUATIONS IN THE $R$ REPRESENTATION

We generalize the treatment of Esbensen and Davids [11], extending it to include the case of nuclei without axial symmetry. Using Eq. 5A-2 of ref. [13], we write the wave function of an odd- $A$  even- $N$  nucleus consisting of a proton coupled to an even-even triaxially-deformed rotor, in the laboratory (space-fixed) system as

$$\Psi_{IM}(\mathbf{r}, \omega) = \sum_{ljR\tau} \frac{\phi_{ljR\tau}^I(r)}{r} |ljR\tau IM\rangle, \quad (1)$$

where  $l$  and  $j$  are the orbital and total angular momentum of the particle,  $R$  and  $\tau$  are the rotational quantum numbers of the rotor, and  $I$  is the total angular momentum of the

nucleus ( $\mathbf{I} = \mathbf{j} + \mathbf{R}$ ). The ket  $|ljR\tau IM\rangle$  describes the dependence on spin and angular coordinates of the particle and the orientation angle of the rotor, and is given by

$$|ljR\tau IM\rangle = \sum_{mM_R} \langle jmRM_R|IM\rangle |R\tau M_R\rangle |ljm\rangle. \quad (2)$$

This is the laboratory frame or R-representation as described in Eq. (2) of ref. [11]. The total Hamiltonian of the proton-core system,

$$H = T + V(\mathbf{r}, \omega) + V_{ls}(\mathbf{r}, \omega) + H_R, \quad (3)$$

consists of the relative kinetic energy  $T$ , the nuclear plus Coulomb interaction  $V(\mathbf{r}, \omega)$ , which depends on the position  $\mathbf{r}$  of the proton and the orientation  $\omega$  of the rotor in the space-fixed system, the deformed spin-orbit potential  $V_{ls}(\mathbf{r}, \omega)$ , and the Hamiltonian  $H_R$  of the rotor. The detailed parametrization of the nuclear and Coulomb interactions are given in Appendix A, and the deformed spin-orbit term is discussed in Appendix B. To proceed, we first expand the potential  $V(\mathbf{r}, \omega)$  in the D-functions, which are related to the spherical harmonics

$$V(\mathbf{r}, \omega) = \sum_{\lambda\mu} V_{\lambda\mu}(r) D_{\mu 0}^{\lambda}(\theta', \phi'), \quad (4)$$

$$V_{\lambda\mu}(r) = \frac{2\lambda+1}{4\pi} \int_{-1}^1 d(\cos\theta') \int_0^{2\pi} d\phi' D_{\mu 0}^{\lambda*}(\theta', \phi') V(r, \theta', \phi'), \quad (5)$$

where  $\theta', \phi'$  refer to the angles of the particle with respect to the 3-axis of the rotor. Because of reflection symmetry,  $\lambda$  and  $\mu$  are restricted to even values (see Appendix A). Projecting with  $|ljR\tau IM\rangle$  on the Schrödinger equation  $H\Psi_{IM} = E\Psi_{IM}$  we obtain a set of coupled equations in the radial wave functions

$$(h_{lj} + E_{R\tau} - E) \phi_{ljR\tau}^I(r) = - \sum_{l'j'R'\tau'} \sum_{\lambda>0,\mu} \langle ljR\tau IM | D_{\mu 0}^{\lambda}(\theta', \phi') | l'j'R'\tau' IM \rangle V_{\lambda\mu}(r) \phi_{l'j'R'\tau'}^I(r) - \sum_{l'j'R'\tau'} \langle ljR\tau IM | V_{ls}(\mathbf{r}, \omega) | l'j'R'\tau' IM \rangle \phi_{l'j'R'\tau'}^I(r), \quad (6)$$

where

$$h_{lj} = \frac{\hbar^2}{2\mu_0} \left( -\frac{d^2}{dr^2} + \frac{l(l+1)}{r^2} \right) + V_0(r),$$

and  $V_0(r)$  is the monopole part of the Coulomb plus nuclear potential. Here  $\mu_0$  is the proton reduced mass, and  $E_{R\tau}$  is the energy of the rotational state  $|R\tau M_R\rangle$ . In Appendix B we will extract the monopole part of the spin-orbit potential for inclusion in  $h_{lj}$ .

### III. THE K REPRESENTATION

The matrix elements on the right hand side of Eq. (6) are easiest to evaluate if we go over into the K-representation of ref. [11], which is oriented in the body-centered coordinates of the rotor. In this system the quantum number  $\tau$  is identified with the projection  $K_R$  of  $R$  on the rotor's 3-axis. For clarity, the quantum numbers  $m$ ,  $M_R$ , and  $M$  in Eq. (2) all refer to angular momentum projections on the z-axis of the space-fixed coordinate system due to the particle, rotor, 3-axis in the body-fixed system are denoted by  $\Omega$ ,  $K_R$ , and  $K$  (see Fig. (1)). As a consequence, the following relations hold:

$$M = M_R + m \quad (7)$$

$$K = K_R + \Omega. \quad (8)$$

In the K-representation we can write the transformed rotor wave function as (see Eq. 4-7 of ref.[13])

$$\langle \omega | R\tau M_R \rangle = \langle \omega | R K_R M_R \rangle = \sqrt{\frac{2R+1}{8\pi^2}} D_{M_R K_R}^R(\omega), \quad (9)$$

which is a function of the orientation  $\omega$  of the rotor in the laboratory frame. For an axially-symmetric rotor, we would have  $K_R = 0$ , resulting in  $\Omega = K$  from Eq. (8). The particle wave function is

$$|ljm\rangle = \sum_{\Omega} D_{m\Omega}^j(\omega) |lj\Omega\rangle, \quad (10)$$

where the single-particle wave function  $|lj\Omega\rangle$  is evaluated in the body-fixed frame of the rotor.

After inserting Eq. (9) and (10) into Eq. (2), we may contract it using Eq. (1A-43) of [13], with the result

$$|ljRK_RIM\rangle = \sqrt{\frac{2R+1}{8\pi^2}} \sum_{K,\Omega} \langle j\Omega R K_R | IK \rangle D_{MK}^I(\omega) |lj\Omega\rangle. \quad (11)$$

Because the rotor possesses symmetry after rotating  $180^\circ$  around any of its three axes, it is convenient to have the projection  $K$  appear only as a positive number. Symmetry properties of the wave function require that the quantity  $K_R = K - \Omega$  be an even integer

$(0, \pm 2, \pm 4 \dots)$  [14]. We then have:

$$|ljRK_RIM\rangle = \sqrt{\frac{2R+1}{8\pi^2}} \sum_{K>0,\Omega} \langle j\Omega RK_R | IK \rangle \left[ D_{MK}^I(\omega) |lj\Omega\rangle + (-1)^{I-j} D_{M-K}^I(\omega) |lj\bar{\Omega}\rangle \right], \quad (12)$$

where  $\bar{\Omega}$  stands for  $-\Omega$ . Since we are only interested in the low-lying states of the rotor where  $R = 0, 2, 4 \dots$ , we rewrite Eq. (12) as

$$|ljRK_RIM\rangle = \sum_{K>0,\Omega} A_{j\Omega,RK_R}^{IK} |lj\Omega KIM\rangle, \quad (13)$$

where

$$A_{j\Omega,RK_R}^{IK} = \sqrt{\frac{2R+1}{2I+1}} \langle j\Omega RK_R | IK \rangle \sqrt{1 + (-1)^R} \quad (14)$$

and

$$|lj\Omega KIM\rangle = \sqrt{\frac{2I+1}{16\pi^2}} \left[ D_{MK}^I(\omega) |lj\Omega\rangle + (-1)^{I-j} D_{M-K}^I(\omega) |lj\bar{\Omega}\rangle \right]. \quad (15)$$

For an axially-symmetric nucleus,  $K_R$  vanishes, making  $\Omega = K$ , and Eq. (14) and (15) become identical to Eq. (14) and (15) of ref. [11].

Inserting Eq. (13) into Eq. (1) we can now express the total wave function in terms of the new basis (15):

$$\Psi_{IM} = \sum_{lj} \sum_{K>0} \sum_{\Omega} \frac{\phi_{lj\Omega}^{IK}(r)}{r} |lj\Omega KIM\rangle, \quad (16)$$

where the radial wave functions are

$$\phi_{lj\Omega}^{IK}(r) = \sum_{RK_R} A_{j\Omega,RK_R}^{IK} \phi_{ljRK_R}^I(r). \quad (17)$$

Note that the triaxial radial wave functions depend on the particle quantum number  $\Omega$  in addition to  $lj$ .

It is easy to show that the amplitudes (14) form an orthonormal transformation between the K and the R representation, i.e.

$$\sum_{K>0} \sum_{\Omega} A_{j\Omega,RK_R}^{IK} A_{j\Omega',RK_R'}^{IK'} = \delta_{R,R'} \delta_{K_R,K_{R'}}, \quad \sum_{RK_R} A_{j\Omega,RK_R}^{IK} A_{j\Omega',RK_R}^{IK'} = \delta_{\Omega,\Omega'} \delta_{K,K'}. \quad (18)$$

Thus we can transform the results obtained in one representation into the other. After inverting Eq. (17) we obtain

$$\phi_{ljRK_R}^I(r) = \sum_{K>0} \sum_{\Omega} A_{j\Omega,RK_R}^{IK} \phi_{lj\Omega}^{IK}(r). \quad (19)$$

### A. Coupled Equations in the $K$ Representation

We continue with the evaluation of the matrix elements on the RHS of Eq. (6). Inserting expression (13) for the spin-angular wave functions in the R-representation we obtain

$$\begin{aligned} \langle ljRK_RIM|D_{\mu 0}^{\lambda}(\theta', \phi')|l'j'R'K_{R'}IM\rangle = \\ \sum_{K>0} \sum_{K'>0} \sum_{\Omega, \Omega'} A_{j\Omega, RK_R}^{IK} \langle lj\Omega KIM|D_{\mu 0}^{\lambda}(\theta', \phi')|l'j'\Omega'K'IM\rangle A_{j'\Omega', R'K_{R'}}^{IK'} \end{aligned}$$

and a similar expression for the matrix element of the spin-orbit potential. The advantage of using the K representation, Eq. (15), now becomes evident because each matrix element is the product of two parts. The first part involves integrating a product of orthogonal D-functions over the orientation coordinates  $\omega$  of the rotor, and yields the important result  $\delta_{K, K'}$ . The second part involves the single-particle wave functions in the body-fixed rest frame of the rotor:

$$\langle lj\Omega|D_{\mu 0}^{\lambda}(\theta', \phi')|l'j'\Omega'\rangle = (-1)^{\lambda} \langle j\frac{1}{2} \lambda 0|j'\frac{1}{2}\rangle \langle j'\Omega' \lambda \mu|j\Omega\rangle. \quad (20)$$

Thus

$$\langle ljRK_RIM|D_{\mu 0}^{\lambda}(\theta', \phi')|l'j'R'K_{R'}IM\rangle = \sum_{K'>0} \sum_{\Omega, \Omega'} A_{j\Omega, RK_R}^{IK'} \langle lj\Omega|D_{\mu 0}^{\lambda}(\theta', \phi')|l'j'\Omega'\rangle A_{j'\Omega', R'K_{R'}}^{IK'}. \quad (21)$$

For the spin-orbit potential we have a similar expression. We show how to evaluate the matrix elements of the spin-orbit interaction in Appendix B. Because the matrix elements are diagonal in  $K$ , Eq. (8) shows that the particle projections  $\Omega, \Omega'$  are restricted by  $|\Omega - \Omega'| =$  an even integer. We still have the previously determined restrictions  $\lambda$  even and  $|K - \Omega| =$  an even integer.

We now obtain the coupled equations in the  $K$  representation by multiplying Eq. (6) by  $A_{j\Omega, RK_R}^{IK}$  and summing over  $RK_R$ , using Eq. (17) and (18). The presence of the rotational energy  $E_{RK_R}$  requires the use of Eq. (19) for the radial wave function. Thus we obtain

$$\begin{aligned} (h_{lj} - E)\phi_{lj\Omega}^{IK}(r) + \sum_{K'>0} \sum_{\Omega'} W_{j\Omega\Omega'}^{KK'} \phi_{lj\Omega'}^{IK'}(r) = \\ - \sum_{l'j'} \sum_{\Omega'} \left\{ \sum_{\lambda>0, \mu} \langle lj\Omega|D_{\mu 0}^{\lambda}(\theta', \phi')|l'j'\Omega'\rangle V_{\lambda\mu}(r) + \langle lj\Omega|V_{ls}(\mathbf{r})|l'j'\Omega'\rangle \right\} \phi_{l'j'\Omega'}^{IK}(r), \quad (22) \end{aligned}$$

where

$$W_{j\Omega\Omega'}^{KK'} = \sum_{RK_R} A_{j\Omega,RK_R}^{IK} E_{RK_R} A_{j\Omega',RK_R}^{IK'}. \quad (23)$$

To recover the axially-symmetric case we set  $\Omega = \Omega' = K$ , and  $\mu = 0$  in Eq. (22) and (23). This removes the sums over  $\Omega'$ ,  $K_R$ , and  $\mu$ .

## B. Adiabatic limit

For a comparison with the results obtained in [11], we will solve the coupled equations (22) in the adiabatic limit, where the rotational energies  $E_{RK_R}$  of the core are set to zero. This sets equal to zero the second term on the left-hand side of Eq. (22). In this case we have

$$(h_{lj} - E)\phi_{lj\Omega}^{IK}(r) = - \sum_{l'j'\Omega'} \left\{ \sum_{\lambda > 0, \mu} \langle lj\Omega | D_{\mu 0}^{\lambda}(\theta', \phi') | l'j'\Omega' \rangle V_{\lambda\mu}(r) + \langle lj\Omega | V_{ls}(\mathbf{r}) | l'j'\Omega' \rangle \right\} \phi_{l'j'\Omega'}^{IK}(r). \quad (24)$$

The important thing to notice is that the coupled equations are then diagonal in  $K$ , but include  $\Omega$ -mixing. In other words, in the adiabatic limit,  $K$  is still a good quantum number, but, in addition to the  $\Omega = K$  component, the interaction mixes into the wave function components with  $\Omega = K \pm 2, K \pm 4$ , etc, subject to the restriction  $|\Omega| \leq j$ . It should also be noted that the Clebsch-Gordan coefficient in Eq. (20) is non-zero only when  $\Omega' + \mu = \Omega$ .

The consequence of this  $\Omega$ -mixing is that the number of coupled equations will be substantially larger than is found in the axially-symmetric case. As an example, consider the combinations of  $j$  and  $\Omega$  needed to solve the equations for the  $I = K = \frac{7}{2}^-$  ground state of the deformed proton emitter  $^{141}\text{Ho}$ . The spherical states involved will be  $j = \frac{7}{2}^-, \frac{9}{2}^-, \frac{11}{2}^-$ ,  $\frac{13}{2}^-$ , and  $\frac{15}{2}^-$ . In addition to  $\Omega = K$ , for each  $j$  there will be associated up to 7 more values of  $\Omega$ . Table I shows the permissible  $j, \Omega$  combinations for the  $I = K = \frac{7}{2}^-$  ground state of  $^{141}\text{Ho}$ . The total number of wave function combinations is 30, which is to be contrasted with only 5 for the axially-symmetric case.

## C. Decay Rate Calculation

We obtain the partial decay rate for proton emission from a state having angular momentum  $I = K$  in the adiabatic limit via either the direct method (Dir) or the distorted

wave Green's function method (DW) using Eq. (7) of [11]. While in the axially-symmetric case the daughter states were labeled only by the quantum number  $R$ , in the triaxial case we need the second label  $\tau$  or  $K_R$  as well:

$$\Gamma_{RK_R}^I = \sum_{lj} \Gamma_{ljRK_R}^I = \frac{\hbar^2 k_R}{\mu} \sum_{lj} |N_{ljRK_R}^{I,Dir/DW}|^2, \quad (25)$$

where

$$\begin{aligned} N_{ljRK_R}^{I,Dir} &= \frac{\phi_{ljRK_R}^I(r)}{G_l(k_R r)} \quad \text{at } r = r_m, \\ N_{ljRK_R}^{I,DW} &= -\frac{2\mu}{\hbar^2 k_R} \sum_{l'j'R'K_{R'}} \int_0^{r_{int}} dr F_l(k_R r) \langle l j R K_R I M | V(\mathbf{r}, \omega) + V_{ls}(\mathbf{r}, \omega) \\ &\quad - \frac{Z_D e^2}{r} | l' j' R' K_{R'} I M \rangle \phi_{l'j'R'K_{R'}}^I(r). \end{aligned} \quad (26)$$

Here  $k_R$  is the proton wave number for the decay to the daughter state with quantum numbers  $RK_R$ . Having obtained the radial wave function  $\phi_{lj\Omega}^{IK}(r)$  for a given  $K = I$  in the adiabatic limit, we can construct the associated radial wave functions in the R representation

$$\phi_{ljRK_R}^I(r) = \sum_{\Omega} A_{j\Omega, RK_R}^{IK} \phi_{lj\Omega}^{IK}(r) \quad (27)$$

by means of Eq. (19). Inserting this wave function into Eq. (26), we obtain for the Direct method

$$N_{ljRK_R}^{I,Dir} = \frac{1}{G_l(k_R r_m)} \sqrt{\frac{2(2R+1)}{2I+1}} \sum_{\Omega} \langle j\Omega R K_R | I K \rangle \phi_{lj\Omega}^{IK}(r_m). \quad (28)$$

Using this equation we can immediately see the effect of the triaxial shape on the decay rate: for decay to the ground state ( $R = 0$ ), the Clebsch-Gordan coefficient has the value  $\delta_{j,I} \delta_{\Omega,K}$ . Thus only the  $\Omega = K$  component of the wave function will participate in this decay branch, effectively reducing its decay rate relative to the that for the axially-symmetric case since there are now other  $\Omega$ -components present in the triaxial wave function.

For the Green's function method, after performing the same operations that led to Eq. (21) to obtain the matrix elements of the interaction in Eq. (26), the second orthogonality relation in Eq. (18) allows the summations over  $R'$  and  $K_{R'}$  to be performed. The final expression for the Green's function method is

$$\begin{aligned} N_{ljRK_R}^{I,DW} &= -\frac{2\mu}{\hbar^2 k_R} \sum_{l'j'} \sum_{\Omega, \Omega'} A_{j\Omega, RK_R}^{IK} \int_0^{r_{int}} dr F_l(k_R r) \langle l j \Omega | V(\mathbf{r}, \omega) + V_{ls}(\mathbf{r}, \omega) \\ &\quad - \frac{Z_D e^2}{r} | l' j' \Omega' \rangle \phi_{l'j'\Omega'}^{IK}(r). \end{aligned} \quad (29)$$

This expression reduces to the analogous one for an axially-symmetric nucleus when  $K$  is set equal to  $\Omega$  and the sums over  $\mu$ ,  $\Omega$  and  $\Omega'$  are removed.

## IV. APPLICATIONS

In this section we use the formalism described above to calculate decay rates for the deformed proton emitter  $^{141}\text{Ho}$  ( $I = K = 7/2^-$ ), in both the axially-symmetric and triaxial cases. The calculations have been performed in the adiabatic limit, using the potential parameters found in ref. [11]. The ground-state wave function was expanded in spherical components with  $j = 7/2^-, 9/2^-, 11/2^-, 13/2^-,$  and  $15/2^-$ . All multipole expansions were carried out up to  $\lambda = 14$ . The results are compared with experimental values for the total decay width and the branching ratio for decay to the first excited  $2^+$  state in the daughter nucleus  $^{140}\text{Dy}$ .

### A. Axially-Symmetric Case: the Deformed Proton Emitter $^{141}\text{Ho}$

To verify the formulation, we have computed the decay half-life and branching ratio to the  $2^+$  state in the daughter nucleus for the deformed proton emitter  $^{141}\text{Ho}$ , using deformed spin-orbit matrix elements for the axially-symmetric case ( $\gamma = \mu = 0$ ,  $\Omega = \Omega' = K$ ) calculated from Eq. (B17), which, again for  $\lambda > 0$ , now reads

$$\langle l j K | V_{ls}(r, \theta) | l' j' K \rangle = 2V_{so} \sum_{\lambda > 0} \frac{\langle j' K \lambda 0 | j K \rangle}{\sqrt{2j+1}} \langle l j \| \left[ \nabla f_{\lambda\mu}(r) D_{\mu 0}^{\lambda}(\hat{\mathbf{r}}) \right] \cdot (-i \nabla \times \hat{\sigma} \| l' j' \rangle, \quad (30)$$

where the reduced matrix element is that calculated in Eq. (B16). The results of the calculations are shown in Table II, and are identical with those obtained using the axially-symmetric deformed spin-orbit term of ref. [11]. It should be noted that the numbers obtained here and in ref. [11] differ slightly, since the  $2^+$  excitation energy of 202 keV in the daughter nuclide  $^{140}\text{Dy}$  used here has only recently been measured [17, 18], and was not known when the calculations in ref. [11] were carried out. In that work an excitation energy of 166 keV was used.

## B. Triaxial Case: the Deformed Proton Emitter $^{141}\text{Ho}$

As previously mentioned, particle-rotor calculations of the energy levels in the rotational band lying above the  $I = 7/2^-$  ground state of the deformed proton emitter  $^{141}\text{Ho}$  were reported in ref. [12]. These calculations suggest that better agreement with experiment would be obtained with the introduction of a small amount of static triaxial deformation. In order to assess the effect on the proton decay rates of adding such a deformation, we have used the formalism developed in the present work to compute, in the adiabatic limit, the decay rate and  $2^+$  branching ratio for this proton emitting nuclide, as a function of the angle of triaxiality  $\gamma$ . The calculations were performed with  $\beta_2 = 0.244$ ,  $\beta_4 = -0.046$ . Preliminary results have been reported in ref. [19].

Fig. 2 shows the product of calculated total decay width  $\Gamma_{calc}$  and spectroscopic factor  $S_{calc} = u^2 = 0.6$  for the  $^{141}\text{Ho}$  ground state, plotted as a function of the triaxial angle  $\gamma$ . The spectroscopic factor was obtained from a BCS calculation, using a proton pairing gap  $\Delta_p$  of 0.9 MeV. The shaded area represents the experimental measurement, and the error bar attached to the calculated curve represents the uncertainty in the calculated width due to the uncertainty in the proton energy. It is seen that calculation and experiment agree well for small values of  $\gamma$ .

Fig. 3 shows the calculated  $2^+$  branching ratio, plotted as a function of  $\gamma$ , along with the experimental value, 0.0070(15) [16]. The small error bar on the calculated curve is due to the uncertainty in the proton energy. The agreement between calculation and experiment is excellent for small values of  $\gamma$ , and this suggests that a static triaxial deformation, if present, is limited to an angle of  $\leq 5^\circ$ .

Plotted in Fig. 4 are the amplitudes for the allowed  $\Omega$ -values of  $+7/2^-$ ,  $+3/2^-$ ,  $-1/2^-$ , and  $-5/2^-$  for the  $j = 7/2$  spherical component of the  $^{141}\text{Ho}$  ground state wave function. As expected, for  $\gamma = 0$ , only the  $\Omega = +7/2^-$  component is present, but with increasing  $\gamma$ , other  $\Omega$ -components differing by  $\pm 2$ ,  $\pm 4 \dots$  begin to mix into the wave function. The decay proceeds primarily to the daughter ground state, and only the  $\Omega = +7/2^-$  component participates in this branch. Thus the decrease in the total decay width with increasing  $\gamma$  seen in Fig. 2 tracks with the decrease in the  $\Omega = +7/2^-$  wave function component, which itself follows from the increasing appearance of other  $\Omega$ -values in the wave function.

## V. CONCLUSIONS

In this work we have developed a formalism to include the effect of static triaxial deformation on calculations of the decay rate for a deformed nucleus. The main complications over the axially-symmetric case are the additional dependence of the interaction potential on the proton azimuthal angle  $\phi$ , and a consequent increase in the complexity of the deformed spin-orbit potential. The extra dimension causes additional  $\Omega$ -components to be introduced into the wave function. The matrix elements of the spin-orbit interaction have been calculated using a tensor algebra approach, as described in Appendix B.

We have applied the abovementioned methodology to calculations of the decay rate of the deformed proton emitter  $^{141g}\text{Ho}$ , which has spin-parity  $7/2^-$ . In ref. [11] it was shown that the non-adiabatic coupled-channels approach does not yield results for  $^{141g}\text{Ho}$  decay which agree with experiment, either for the absolute decay rate or the branching ratio for decay to the first  $2^+$  of the daughter nucleus  $^{140}\text{Dy}$ . This is because of the presence of Coriolis mixing, which is particularly strong for high spin states. Empirically it is known that it is necessary to quench the Coriolis mixing in order to obtain good agreement with data [20, 21]. It was found in [11] that good agreement with experiment was obtained in the adiabatic limit, where the energies of the rotational states of the daughter nucleus are set to zero. For this reason we have performed the triaxial calculations in the adiabatic limit.

After first checking the results of the calculation against an axially-symmetric code, triaxiality was introduced, ranging up to a  $\gamma$  angle of  $40^\circ$ . While the sensitivity of the resulting total decay rate to triaxial angle  $\gamma$  was not high, the calculation of the branching ratio for decay to the first  $2^+$  state of the daughter showed a strong dependence on  $\gamma$ , essentially ruling out angles greater than  $5^\circ$ . We believe that the branching ratio calculation is quite reliable, since factors such as absolute spectroscopic factors tend to cancel.

In conclusion, we do not believe that a static triaxial deformation plays an important role in helping to explain the decay rate of the deformed proton emitter  $^{141g}\text{Ho}$ . Triaxiality may still exert an influence on the nuclear structure of this nuclide, but most likely at higher spins and excitation energies.

## Acknowledgments

This work was supported by the U. S. Department of Energy, Nuclear Physics Division, under Contract No. W-31-109-ENG-38.

## APPENDIX A: PARAMETRIZATION OF THE INTERACTION POTENTIAL

For triaxial nuclei, the degree of triaxiality is denoted by the angle  $\gamma$ , which is one of the Hill-Wheeler [22] coordinates. We parametrize the nuclear interaction between the valence proton and the deformed core nucleus in terms of the Fermi function  $f(x) = [1 + \exp(x)]^{-1}$  as

$$V_N(r, \theta, \phi) = V_N^{(0)} f\left(\frac{r - R(\theta, \phi)}{a(\theta)}\right), \quad (\text{A1})$$

where  $V_N^{(0)}$  is the depth of the nuclear potential,  $a(\theta)$  is an angle-dependent diffuseness as in Eq. (A6) of [11], and

$$R(\theta, \phi) = R_N \left\{ 1 + \sum_{\mu=-2, even}^2 a_{2\mu} Y_{2\mu}(\theta, \phi) + \sum_{\mu=-4, even}^4 a_{4\mu} Y_{4\mu}(\theta, \phi) \right\}. \quad (\text{A2})$$

Here  $(\theta, \phi)$  are the angles between  $\mathbf{r}$  and the 3-axis of the core, and

$$\begin{aligned} a_{20} &= \beta_2 \cos \gamma & a_{22} &= a_{2-2} = \frac{\beta_2 \sin \gamma}{\sqrt{2}} \\ a_{40} &= \frac{1}{6} \beta_4 (5 \cos^2 \gamma + 1) \\ a_{42} &= a_{4-2} = -\frac{1}{12} \beta_4 \sqrt{30} \sin 2\gamma \\ a_{44} &= a_{4-4} = \frac{1}{12} \beta_4 \sqrt{70} \sin^2 \gamma. \end{aligned} \quad (\text{A3})$$

The radius is calculated as

$$R_N = r_0 \left( \frac{A_D}{C(\beta_2, \beta_4, \gamma)} \right)^{\frac{1}{3}}, \quad (\text{A4})$$

where

$$C(\beta_2, \beta_4) = \int \frac{d\Omega}{4\pi} \left( 1 + \sum_{\mu=-2, even}^2 a_{2\mu} Y_{2\mu}(\theta, \phi) + \sum_{\mu=-4, even}^4 a_{4\mu} Y_{4\mu}(\theta, \phi) \right)^3 \quad (\text{A5})$$

is the volume preserving factor and  $A_D$  is the mass number of the core. Equations (A2) and (A5) reduce to Eq. (A1) and (A2) of [11] for the axially-symmetric case ( $\mu = \gamma = 0$ ). Values of  $r_0 = 1.25$  fm and  $a = 0.65$  fm are used in our calculations.

We parametrize the charge density of the core in a similar way, using the slightly different radial parameters of  $r_0 = 1.22$  fm and  $a_C = 0.56$  fm, as was done in ref. [11].

## APPENDIX B: DEFORMED SPIN-ORBIT POTENTIAL

For the solution of the coupled equations Eq. (24), matrix elements of the spin-orbit potential  $\langle lj\Omega|V_{ls}(r, \theta, \phi)|l'j'\Omega'\rangle$  are needed. As in ref. [11] we use a deformed spin-orbit potential, but with the addition of  $\phi$ -dependent terms not found there. We follow the tensor algebra approach of Hagino [23], who has calculated matrix elements of the spin-orbit interaction in the context of particle-vibration coupling for spherical nuclei.

The starting point is to express the deformed spin-orbit interaction in the Thomas form [11] with the deformed Fermi function of Eq. (A1):

$$V_{ls}(r, \theta, \phi) = 4V_{so} \left( \left[ \nabla f \left( \frac{r - R(\theta, \phi)}{a} \right) \right] \times \mathbf{p} \cdot \mathbf{s} \right). \quad (\text{B1})$$

We now make a multipole expansion of the Fermi function

$$f(r, \theta, \phi) = \sum_{\lambda\mu} f_{\lambda\mu}(r) D_{\mu 0}^{\lambda}(\hat{\mathbf{r}}), \quad (\text{B2})$$

$$\begin{aligned} f_{\lambda\mu}(r) &= \frac{2\lambda + 1}{4\pi} \int D_{\mu 0}^{\lambda*}(\hat{\mathbf{r}}) f(r, \theta, \phi) d(\cos\theta) d\phi, \\ \frac{df_{\lambda\mu}(r)}{dr} &= \frac{2\lambda + 1}{4\pi} \int D_{\mu 0}^{\lambda*}(\hat{\mathbf{r}}) \frac{df(r, \theta, \phi)}{dr} d(\cos\theta) d\phi. \end{aligned} \quad (\text{B3})$$

So

$$\begin{aligned} V_{ls}(r, \theta, \phi) &= 4V_{so} \left( \sum_{\lambda\mu} \left[ \nabla f_{\lambda\mu}(r) D_{\mu 0}^{\lambda}(\hat{\mathbf{r}}) \right] \times \mathbf{p} \cdot \mathbf{s} \right) \\ &= 4V_{so} \left( \frac{1}{r} \frac{df_{00}(r)}{dr} D_{00}^0(\hat{\mathbf{r}}) (\mathbf{r} \times \mathbf{p}) \cdot \mathbf{s} + \sum_{\lambda > 0, \mu} \left[ \nabla f_{\lambda\mu}(r) D_{\mu 0}^{\lambda}(\hat{\mathbf{r}}) \right] \times \mathbf{p} \cdot \mathbf{s} \right) \\ &= 4V_{so} \left( \frac{1}{r} \frac{df_{00}(r)}{dr} \mathbf{l} \cdot \mathbf{s} + \frac{1}{2} \sum_{\lambda > 0, \mu} \left[ \nabla f_{\lambda\mu}(r) D_{\mu 0}^{\lambda}(\hat{\mathbf{r}}) \right] \cdot (-i\nabla \times \hat{\sigma}) \right) \end{aligned} \quad (\text{B4})$$

The first term on the RHS of Eq. (B4) is the monopole part of the spin-orbit potential,

$$V_{ls}^0(r) = 4V_{so} \frac{1}{r} \frac{df_{00}(r)}{dr} \mathbf{l} \cdot \mathbf{s}, \quad (\text{B5})$$

which can easily be incorporated into the monopole part of the Hamiltonian. The second term,

$$\delta V_{ls}(r, \theta, \phi) = V_{ls}(r, \theta, \phi) - V_{ls}^0(r), \quad (\text{B6})$$

can be decomposed into a sum of angular momentum tensors involving the spherical harmonics  $Y_{\lambda\mu}(\hat{\mathbf{r}})$ , using the gradient formula Eq. (5.9.17) of [24]:

$$\left[ \nabla f_{\lambda\mu}(r) D_{\mu 0}^{\lambda}(\hat{\mathbf{r}}) \right] \cdot (-i\nabla \times \hat{\sigma}) = -\frac{\sqrt{4\pi(\lambda + 1)}}{2\lambda + 1} \left( \frac{df_{\lambda\mu}(r)}{dr} - \frac{\lambda}{r} f_{\lambda\mu}(r) \right) [Y_{\lambda+1}(-i\nabla \times \hat{\sigma})]^{\lambda\mu}$$

$$\begin{aligned}
& + \frac{\sqrt{4\pi\lambda}}{2\lambda+1} \left( \frac{df_{\lambda\mu}(r)}{dr} + \frac{\lambda+1}{r} f_{\lambda\mu}(r) \right) [Y_{\lambda-1}(-i\nabla \times \hat{\sigma})]^{\lambda\mu} \\
& = \frac{\sqrt{4\pi}}{2\lambda+1} \left\{ \sqrt{\lambda} Q_{\lambda\mu}(r) T_-^{\lambda\mu} - \sqrt{\lambda+1} P_{\lambda\mu}(r) T_+^{\lambda\mu} \right\}, \quad (B7)
\end{aligned}$$

where

$$\begin{aligned}
T_{\pm}^{\lambda\mu} &= [Y_{\lambda\pm 1}(-i\nabla \times \hat{\sigma})]^{\lambda\mu}, \quad (B8) \\
P_{\lambda\mu}(r) &= \frac{df_{\lambda\mu}(r)}{dr} - \frac{\lambda}{r} f_{\lambda\mu}(r), \quad \text{and} \\
Q_{\lambda\mu}(r) &= \frac{df_{\lambda\mu}(r)}{dr} + \frac{\lambda+1}{r} f_{\lambda\mu}(r).
\end{aligned}$$

To solve the coupled radial equations we need to obtain the matrix elements of the operator  $\sum_{\lambda>0,\mu} [\nabla f_{\lambda\mu}(r) D_{\mu 0}^{\lambda}(\hat{\mathbf{r}})] \cdot (-i\nabla \times \hat{\sigma})$ , or specifically, the matrix elements of  $\sum_{\lambda>0,\mu} T_{\pm}^{\lambda\mu}$  between spin-angular momentum states. This is done by using the Wigner-Eckart theorem

$$\langle lj\Omega | T_{\pm}^{\lambda\mu} | l'j'\Omega' \rangle = \langle j'\Omega' \lambda\mu | j\Omega \rangle \frac{\langle lj \| T_{\pm}^{\lambda} \| l'j' \rangle}{\sqrt{2j+1}} \quad (B9)$$

along with reduced matrix elements given in Eq. (58) and (59) of ref. [25] and Eq. (A2.14) of ref. [26]. Eq. (B9) is the point of departure between axially-symmetric and triaxial calculations of the spin-orbit matrix elements, since the reduced matrix elements are independent of the projection quantum numbers  $\Omega'$ ,  $\Omega$ , and  $\mu$ . For axial symmetry we will set  $\Omega = \Omega' = K$  and  $\gamma = \mu = 0$ .

Putting  $L_{\pm} = \lambda \pm 1$  we have

$$\begin{aligned}
\langle lj \| T_{\pm}^{\lambda} \| l'j' \rangle &= \langle lj \| [Y_{L_{\pm}}(-i\nabla \times \hat{\sigma})]^{\lambda} \| l'j' \rangle \\
&= \sum_{l_{\alpha}j_{\alpha}} (-1)^{\lambda+j+j'+1} \sqrt{36(2\lambda+1)(2j'+1)(2j_{\alpha}+1)} \\
&\quad \times \left\{ \begin{array}{ccc} L_{\pm} & 1 & \lambda \\ j' & j & j_{\alpha} \end{array} \right\} \left\{ \begin{array}{ccc} l_{\alpha} & l' & 1 \\ \frac{1}{2} & \frac{1}{2} & 1 \\ j_{\alpha} & j' & 1 \end{array} \right\} \langle lj \| Y_{L_{\pm}} \| l_{\alpha}j_{\alpha} \rangle \langle Y_{l_{\alpha}} \| \nabla \| Y_{l'} \rangle, \quad (B10)
\end{aligned}$$

where

$$\langle lj \| Y_{L_{\pm}} \| l_{\alpha}j_{\alpha} \rangle = (-1)^{\frac{1}{2}+j} \sqrt{\frac{(2j+1)(2L_{\pm}+1)(2j_{\alpha}+1)}{4\pi}} \left( \begin{array}{ccc} j & L_{\pm} & j_{\alpha} \\ \frac{1}{2} & 0 & -\frac{1}{2} \end{array} \right) \quad (B11)$$

and

$$\langle Y_{l_{\alpha}} \| \nabla \| Y_{l'} \rangle = \sqrt{2l'+1} \langle l'010 | l_{\alpha}0 \rangle \left[ \frac{d}{dr} + \frac{1}{r} + \frac{1}{2r} \{ l'(l'+1) - l_{\alpha}(l_{\alpha}+1) \} \right]. \quad (B12)$$

From the properties of the Clebsch-Gordan coefficient in Eq. (B12) it can be seen that  $l_\alpha$  can take on only the 2 values  $l' \pm 1$ , indicating that the parity of  $l_\alpha j_\alpha$  is opposite to that of  $l' j'$  and  $l j$ . The permissible values of  $j_\alpha$  in the summation in Eq. (B10) are  $j_\alpha = l_\alpha \pm 1/2$ , and may be further restricted by the triangle relations for the 6j-symbol, namely  $\Delta(L_\pm j j_\alpha)$  and  $\Delta(j' 1 j_\alpha)$ . Additionally, for the calculation of the matrix elements, the  $d/dr$  term in Eq. (B12) needs to be modified, since the coupled equations are in the wave function  $\phi_l(r)$ , while the Hamiltonian (3) acts on the wave function (1), which contains  $\phi_l(r)/r$ . Since

$$r \frac{d}{dr} \left( \frac{\phi_l(r)}{r} \right) = \frac{d\phi_l(r)}{dr} - \frac{\phi_l(r)}{r}, \quad (\text{B13})$$

we see that the operator  $d/dr$  must be replaced by  $(d/dr - 1/r)$  in the coupled equations for  $\phi_l(r)$ . This replacement has been performed below.

Finally, after noting that  $\lambda$  is always even in this application, we have

$$\frac{\sqrt{4\pi}}{2\lambda + 1} \langle l j \| T_\pm^\lambda \| l' j' \rangle = C^\lambda(j' j L_\pm) \sum_{l_\alpha j_\alpha} A^\lambda(j_\alpha j' j L_\pm) \left[ \frac{d}{dr} + \frac{1}{2r} \{ l'(l' + 1) - l_\alpha(l_\alpha + 1) \} \right], \quad (\text{B14})$$

where

$$C^\lambda(j' j L_\pm) = (-1)^{j'+\frac{1}{2}} \sqrt{\frac{36(2j'+1)(2L_\pm+1)(2j+1)(2l'+1)}{(2\lambda+1)}}, \quad (\text{B15})$$

and

$$A^\lambda(j_\alpha j' j L_\pm) = (2j_\alpha + 1) \left\{ \begin{array}{ccc} L_\pm & 1 & \lambda \\ j' & j & j_\alpha \end{array} \right\} \left\{ \begin{array}{ccc} l_\alpha & l' & 1 \\ \frac{1}{2} & \frac{1}{2} & 1 \\ j_\alpha & j' & 1 \end{array} \right\} \left( \begin{array}{ccc} j & L_\pm & j_\alpha \\ \frac{1}{2} & 0 & -\frac{1}{2} \end{array} \right) \langle l' 0 1 0 | l_\alpha 0 \rangle.$$

After some rearrangement, we can write the reduced matrix element of the operator  $[\nabla f_{\lambda\mu}(r) D_{\mu 0}^\lambda(\hat{\mathbf{r}})] \cdot (-i\nabla \times \hat{\sigma})$  as

$$\begin{aligned} \langle l j \| [\nabla f_{\lambda\mu}(r) D_{\mu 0}^\lambda(\hat{\mathbf{r}})] \cdot (-i\nabla \times \hat{\sigma} \| l' j' \rangle = & \left\{ \sqrt{\lambda} Q_{\lambda\mu}(r) C^\lambda(j' j L_-) \sum_{l_\alpha j_\alpha} A^\lambda(j_\alpha j' j L_-) - \sqrt{\lambda+1} P_{\lambda\mu}(r) C^\lambda(j' j L_+) \sum_{l_\alpha j_\alpha} A^\lambda(j_\alpha j' j L_+) \right\} \frac{d}{dr} \\ & + \frac{1}{2r} \left\{ \sqrt{\lambda} Q_{\lambda\mu}(r) C^\lambda(j' j L_-) \sum_{l_\alpha j_\alpha} A^\lambda(j_\alpha j' j L_-) [l'(l'+1) - l_\alpha(l_\alpha+1)] \right\} \\ & - \frac{1}{2r} \left\{ \sqrt{\lambda+1} P_{\lambda\mu}(r) C^\lambda(j' j L_+) \sum_{l_\alpha j_\alpha} A^\lambda(j_\alpha j' j L_+) [l'(l'+1) - l_\alpha(l_\alpha+1)] \right\}. \end{aligned} \quad (\text{B16})$$

Recall that our original goal is to compute the spin-angular coupling matrix elements of the deformed spin-orbit interaction. For  $\lambda > 0$  we have, from Eqs. (B4) and (B9),

$$\langle l j \Omega | \delta V_{ls}(r, \theta, \phi) | l' j' \Omega' \rangle = 2V_{so} \sum_{\lambda > 0, \mu} \frac{\langle j' \Omega' \lambda \mu | j \Omega \rangle}{\sqrt{2j + 1}} \langle l j \| \left[ \nabla f_{\lambda \mu}(r) D_{\mu 0}^{\lambda}(\hat{\mathbf{r}}) \right] \cdot (-i \nabla \times \hat{\sigma} \| l' j' \rangle. \quad (\text{B17})$$

---

[1] P. J. Woods and C. N. Davids, *Annu. Rev. Nucl. Part. Sci.* **47**, 541 (1997).

[2] P. Möller et al., *At. Data Nucl. Data Tables* **59**, 185 (1995).

[3] V. P. Bugrov and S. G. Kadmensky, *Sov. J. Nucl. Phys.* **49**, 967 (1989).

[4] S. G. Kadmensky and V. P. Bugrov, *Phys. At. Nucl.* **59**, 399 (1996).

[5] L. S. Ferreira, E. Maglione, and R. J. Liotta, *Phys. Rev. Lett.* **78**, 1640 (1997).

[6] E. Maglione, L. S. Ferreira, and R. J. Liotta, *Phys. Rev. Lett.* **81**, 538 (1998).

[7] E. Maglione, L. S. Ferreira, and R. J. Liotta, *Phys. Rev. C* **59**, R589 (1999).

[8] A. A. Sonzogni et al., *Phys. Rev. Lett.* **83**, 1116 (1999).

[9] A. T. Kruppa et al., *Phys. Rev. Lett.* **84**, 4549 (2000).

[10] B. Barmore et al., *Phys. Rev. C* **62**, 054315 (2000).

[11] H. Esbensen and C. N. Davids, *Phys. Rev. C* **63**, 014315 (2001).

[12] D. Seweryniak et al., *Phys. Rev. Lett.* **86**, 1458 (2001).

[13] A. Bohr, B. R. Mottelson, “*Nuclear Structure*”, Vol. II (W. A. Benjamin, Reading, 1975).

[14] A. Bohr, *Mat. Fys. Medd. Dan. Vid. Selsk.* **26**, No. 14 (1952).

[15] C. N. Davids et al., *Phys. Rev. Lett.* **80**, 1849 (1998).

[16] K. Rykaczewski et al., Proc. of Int. Conf. on Nucl. Structure ”Mapping the Triangle”, Grand Teton National Park, Wyoming, 22-25 May 2002, AIP Proceedings 638, 149 (2002).

[17] D. Cullen et al., *Phys. Lett. B* **529**, 42 (2002).

[18] W. Królas et al., *Phys. Rev. C* **65**, 031303 (2002).

[19] C. N. Davids and H. Esbensen, Proceedings of the 2nd International Symposium on Proton-Emitting Nuclei, Ed. E. Maglione and F. Soramel,(AIP Press) 41, 2003.

[20] A. Henriquez, T. Engeland, and J. Rekstad, *Phys. Rev. C* **27**, 1302 (1983).

[21] G. Fiorin, E. Maglione, and L. S. Ferreira, *Phys. Rev. C* **67**, 054302 (2003).

[22] D. L. Hill and J. A. Wheeler, *Phys. Rev.* **89**, 1102 (1953).

[23] K. Hagino, *Phys. Rev. C* **64**, 041304(R) (2001).

[24] A. R. Edmonds, “Angular Momentum in Quantum Mechanics”, Princeton University Press (1974).

[25] P.-G. Reinhard and Y. K. Gambhir, *Ann. Phys. (Leipzig)* **1**, 598 (1992).

[26] R. D. Lawson, “Theory of the Nuclear Shell Model”, Oxford University Press (1980).

TABLE I: Combinations of  $j$  and  $\Omega$  for  $I = K = \frac{7}{2}^-$  originating from  $j = \frac{7}{2}^- \rightarrow \frac{15}{2}^-$ . The bullet (•) denotes states occurring in the axially-symmetric case.

$j$	$\Omega$	Axially-Symmetric	$j$	$\Omega$	Axially-Symmetric
$\frac{7}{2}^-$	$-\frac{5}{2}$		$\frac{13}{2}^-$	$-\frac{13}{2}$	
$\frac{7}{2}^-$	$-\frac{1}{2}$		$\frac{13}{2}^-$	$-\frac{9}{2}$	
$\frac{7}{2}^-$	$\frac{3}{2}$		$\frac{13}{2}^-$	$-\frac{5}{2}$	
$\frac{7}{2}^-$	$\frac{7}{2}$	•	$\frac{13}{2}^-$	$-\frac{1}{2}$	
$\frac{9}{2}^-$	$-\frac{9}{2}$		$\frac{13}{2}^-$	$\frac{3}{2}$	
$\frac{9}{2}^-$	$-\frac{5}{2}$		$\frac{13}{2}^-$	$\frac{7}{2}$	•
$\frac{9}{2}^-$	$-\frac{1}{2}$		$\frac{13}{2}^-$	$\frac{11}{2}$	
$\frac{9}{2}^-$	$\frac{3}{2}$		$\frac{15}{2}^-$	$-\frac{13}{2}$	
$\frac{9}{2}^-$	$\frac{7}{2}$	•	$\frac{15}{2}^-$	$-\frac{9}{2}$	
$\frac{11}{2}^-$	$-\frac{9}{2}$		$\frac{15}{2}^-$	$-\frac{5}{2}$	
$\frac{11}{2}^-$	$-\frac{5}{2}$		$\frac{15}{2}^-$	$-\frac{1}{2}$	
$\frac{11}{2}^-$	$-\frac{1}{2}$		$\frac{15}{2}^-$	$\frac{3}{2}$	
$\frac{11}{2}^-$	$\frac{3}{2}$		$\frac{15}{2}^-$	$\frac{7}{2}$	•
$\frac{11}{2}^-$	$\frac{7}{2}$	•	$\frac{15}{2}^-$	$\frac{11}{2}$	
$\frac{11}{2}^-$	$\frac{11}{2}$		$\frac{15}{2}^-$	$\frac{15}{2}$	

TABLE II: Comparison of calculated and experimental values for  $^{141}\text{Ho}(7/2^-)$  total decay rate and  $2^+$  branching ratio. Input values are:  $E_x(2^+)$  in  $^{140}\text{Dy} = 202$  keV,  $\beta_2 = 0.244$ , and  $\beta_4 = -0.046$ . Calculations were done in the adiabatic limit, with no static triaxiality, and uncertainties coming from the measured proton energy of 1169(8) keV [15] and the decay half-life of 4.2(4) ms [15] have been taken into account. The experimental spectroscopic factor  $S_{exp}$  is defined as  $\Gamma_{exp}/\Gamma_{calc}$ . The calculated spectroscopic factor  $S_{calc} = u^2$  is obtained from a BCS calculation (see text).

$\Gamma_{calc}$ ( $10^{-19}$ MeV)	$\Gamma_{exp}$ ( $10^{-19}$ MeV)	$S_{calc}$	$S_{exp}$	$BR(2^+)_{calc}$	$BR(2^+)_{exp}$
$1.51^{+.34}_{-.28}$	$1.09(10)^a$	0.6	$0.72^{+.17}_{-.15}$	0.0071(5)	$0.0070(15)^b$

<sup>a</sup>Ref. [15]

<sup>b</sup>Ref. [16]

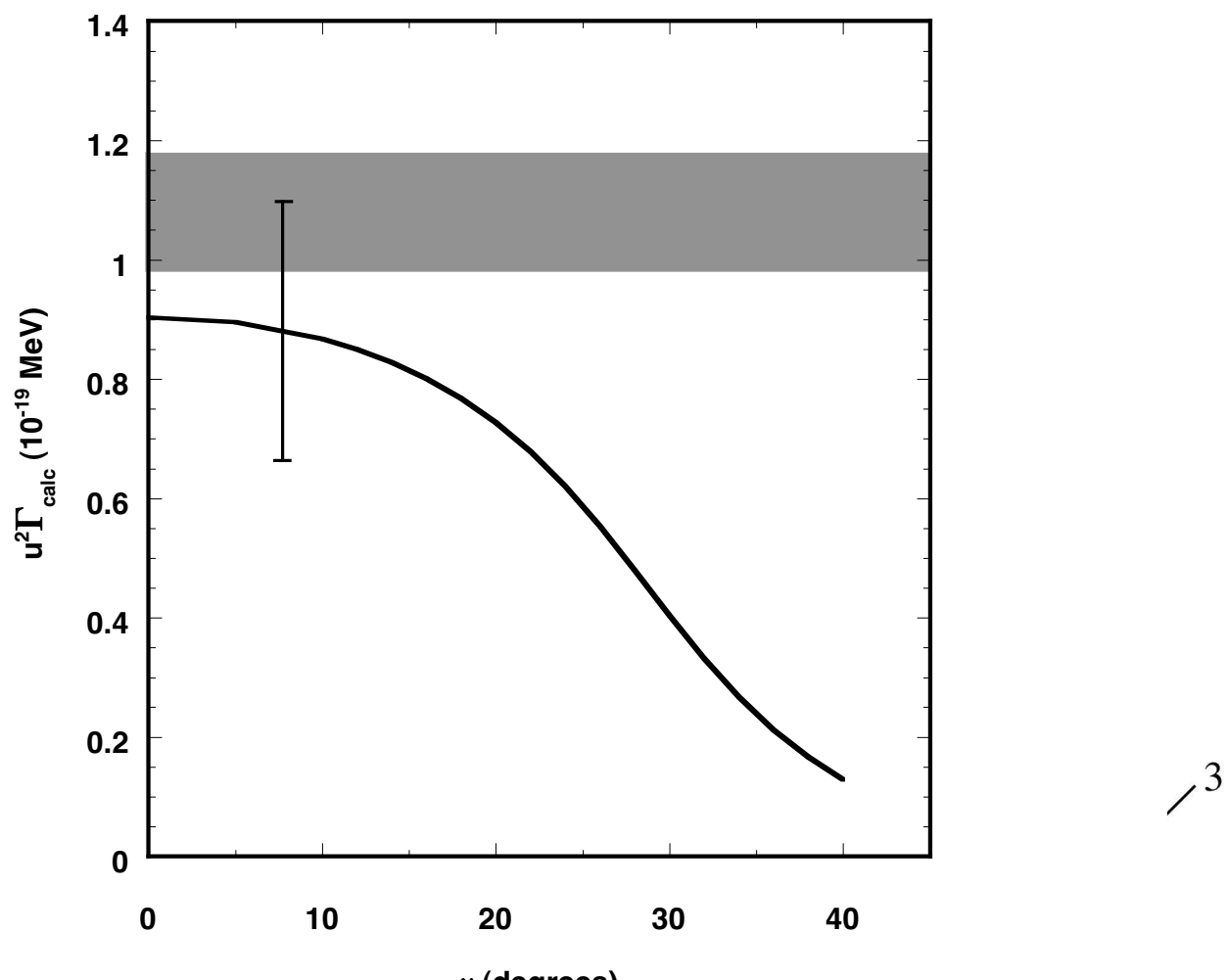
FIG. 1: (a) Relationship of the angular momentum vectors  $\mathbf{j}$ ,  $\mathbf{R}$ , and  $\mathbf{I}$  in the axially-symmetric case. (b) Same as (a) except for the triaxial case. In both cases  $K$  is the projection of the total angular momentum  $\mathbf{I}$  on the 3-axis of the body-centered system.

FIG. 2: Calculated total decay width, in units of  $10^{-19}$  MeV, for  $^{141g}\text{Ho}$ , plotted as a function of the triaxial angle  $\gamma$ . The shaded area represents the experimental measurement, and the error bar attached to the calculated curve represents the uncertainty in the calculated width due to the uncertainty in the proton energy.

FIG. 4: Amplitudes for various  $\Omega$ -values of the  $j = 7/2^-$  component of the  $^{141g}\text{Ho}$  wave function, plotted as a function of the triaxial angle  $\gamma$ .

FIG. 3: Calculated branching ratio in percent for the decay of  $^{141g}\text{Ho}$  to the  $2^+$  state of  $^{140}\text{Dy}$  at an excitation energy of 202 keV, plotted as a function of the triaxial angle  $\gamma$ . The shaded area represents the experimental measurement, and the error bar attached to the calculated curve represents the uncertainty in the calculated branching ratio due to the uncertainty in the proton energy.

**$^{141g}\text{Ho}$  Proton Decay Width vs. Triaxiality**



$$K = \Omega + K_R$$

